Hypersalinity drives convergent bone mass increases in Miocene marine mammals from the Paratethys

Leonard Dewaele, Pavel Gol'din, Felix Marx, Olivier Lambert, Michel Laurin, Theodor Obadă, Vivian de Buffrénil

Hypersalinity drives convergent bone mass increases in Miocene marine mammals

Authors: Leonard Dewaele[1,2,*], Pavel Gol'din[3,4], Felix G. Marx[5,6], Olivier Lambert[2], Michel Laurin[7], Theodor Obadă[8], and Vivian de Buffrénil[7]

[1]EDDy Lab, Department of Geology, Liège University, Quartier Agora, 14 Allée du six Août, Liège 4000, Belgium.

[2]Directorate Earth and History of Life, Royal Belgian Institute of Natural Sciences, 29 Rue Vautier, Brussels 1000, Belgium.

[3]Schmalhausen Institute of Zoology, National Academy of Sciences of Ukraine, vul. Bogdana Khmelnytskogo 15, Kyiv 01030, Ukraine

[4]Ukrainian Scientific Centre of Ecology of the Sea, Frantsuzsky Blvrd. 89, Odessa 65009, Ukraine.

[5]Museum of New Zealand Te Papa Tongarewa, 169 Tory Street, Wellington 6011, New Zealand.

[6]Department of Geology, University of Otago, 360 Leith Walk, Dunedin 9054, New Zealand.

[7]UMR 7207 (CNRS/MNHN/UPMC, Sorbonne Universités), «Centre de Recherches de Paléontologie – Paris», Muséum National d'Histoire Naturelle, Paris 75005, France.

[8]Institute of Zoology, Academy of Sciences of Moldova, str. Academiei, 1 MD-2028, Chișinău, Moldova.

*Corresponding author and lead contact

Author contact: LD: ldewaele@uliege.be; PG: pavelgoldin412@gmail.com; FGM: felix.marx@tepapa.govt.nz; OL: olambert@naturalsciences.be; ML: michel.laurin@mnhn.fr; TO: theodorobada@gmail.com; VB: vivian.de-buffrenil@mnhn.fr.

SUMMARY

Pachyosteosclerosis – dense, bulky bones – often characterizes the early evolution of secondarily aquatic tetrapods like whales and dolphins [1-3], but then usually fades away as swimming efficiency increases [4]. Here, we document a remarkable reversal of this pattern, namely, the convergent re-emergence of bone densification in Miocene seals, dolphins and whales from the epicontinental Paratethys Sea of Eastern Europe and Central Asia. This phenomenon was driven by imbalanced remodeling and inhibited resorption of primary trabeculae, and coincided with hypersaline conditions the Badenian Salinity Crisis that affected the Central Paratethys between 13.8 and 13.4 Ma [5]. Dense bones acting as ballast would have facilitated efficient swimming in the denser and more buoyant water, and hence were likely adaptive in this setting. From the Central Paratethys, pachyosteosclerosis subsequently spread eastward, where it became a defining feature of the endemic late Miocene whale assemblage [6,7].

Keywords: Cetacea, Phocidae, Paratethys, Miocene, Osteohistology, Microanatomy, Hypersalinity, Paleoceanography

RESULTS

Relative bone dimensions and compactness in seven true seals (phocids), two baleen whales (mysticetes), and two toothed whales (odontocetes) from the Miocene of the Paratethys (Figures 1, S1; Table S1) show that osteosclerosis was pervasive, while pachyostosis characterized the cetaceans only.

Pachyostosis

Pronounced pachyostosis, i.e. thickening of the bones, occurs in both the putative platanistid dolphin *Pachyacanthus* from the Central Paratethys and the two cetotheriine mysticetes from the Eastern Paratethys (Figure 2A-E). By contrast, the limb bones of Paratethyan true seals (Figure 2F, G) resemble, or are more gracile than, those of their living cousins, as judged by their overall 'Bulkiness Index' [10] (Tables S2, S3). The lack of pachyostosis in seals is not due to crushing, as none of the specimens we examined showed notable volumes of cancellous bone. In addition, bulkiness does not appear to be correlated with individual size; it may hence be diagnostic of particular species. Owing to a lack of data, we cannot rule out gender as a biasing variable.

Microanatomy

We prepared thin sections to quantify the relative area (in %) occupied by bone tissue (global compactness, Cg), as well as the relative width of the transition zone between the medulla and the cortex (S); the distance of this transition zone from the center of the sections (P); and the minimum (Min) and maximum (Max) values of bone compactness [11].

In general, the limb bones of Paratethyan seals are highly compact (Cg = 97–100%), with no medullary cavity or extensive cancellous core (Figures 2H-N, S2, Table S4). They typically

show low values of S, and small differences between Min and Max. Transverse and sagittal sections reveal extreme osteosclerosis affecting the entire bone (Figures 2, S2; Table S4), including regions (i.e. metaphyses and epiphyses) normally occupied by relatively loose cancellous formations [12]. Other phocids, including extant species, have a broad and well-differentiated medullary cavity and compactness indices <70% (Table S4).

Like their pinniped contemporaries, Paratethyan cetaceans possess highly compact, amedullary bones (Figure 2B-E). The latter are notably more osteosclerotic than those of both extant whales and dolphins and, surprisingly, Eocene stem cetaceans like *Rodhocetus* and *Dorudon* (Table S4). Even in the least compact specimens (Cg = 99.4–99.8%), inner bone porosity is limited to small, scattered cavities less than 500 µm in diameter.

Osteohistology

The medullary region in all of our Paratethyan seals consists of an extremely remodeled, compacted spongiosa (Figure 3A, B). Under polarized light, the local bone structure is complex and irregular, with remnants of endosteal trabeculae, thick endosteal layers of lamellar tissue filling former intertrabecular spaces, and variably oriented secondary osteons. There are no traces of calcified cartilage matrix. Haversian remodeling remains local and broad areas of primary periosteal tissue, consisting of a woven-parallel complex with longitudinal, oblique, circular or radial primary osteons, persist in the cortex (Figure 3C-F). Laminar organization is the most frequent and best characterized, especially in deep cortices (Figure 3C, F), but a single section may display a combination of several vascular patterns (e.g., Figure 3C, D, F), including (generally longitudinal) secondary osteons.

In *Sarmatonectes*, *Praepusa* and *Pachyphoca*, the laminar tissue in the deep cortex is abruptly replaced by thick layers with a mostly radial vascular pattern (Figure 3C, D, F). Towards the

periphery, primary osteons become sparser and oriented longitudinally before ultimately disappearing in the outermost layers. Where preserved, the latter often consist of parallel-fibered or lamellar tissues, which suggests the end of local skeletal growth (Figure 3B, E, H). However, the periphery of the *Pachyphoca* humerus (Figure 3F) consists of reticular tissue, which shows that the individual was still actively growing shortly before it died.

Most specimens display sharp (Figure 3C, D) or diffuse (Figure 3E-G) annuli made of parallel-fibered tissue, along with lines of arrested growth (Figure 3 H). Sharpey's fibres, generally located within the annuli, are also common. The growth in diameter of both the humeri and the femora was strongly asymmetrical, with active accretion occurring on the lateral face of the shaft, while the medial face either grew slowly or was under resorption.

Among our sample of cetaceans, all species share a similar structure of the cortex, but the delphinidan humerus differs from the ribs of the cetotheriines and *Pachyacanthus* in the characteristics of the medullary region.

In the ribs, the medulla is extremely remodeled and completely filled with thick endosteal lamellar tissue (Figure 4A). Secondary osteons are mostly longitudinal, and spread to the detriment of the endosteal deposits and neighboring strata of the cortex (Figure 4B). The primary cortex consists of a plexiform woven-parallel complex that may locally turn into the laminar type (Figure 4C, D). Longitudinal primary osteons often occur alongside circular ones. In the outer cortex, periosteal deposits tend to turn into parallel-fibered tissue vascularized by few simple, longitudinal canals. Secondary osteons are scarce at this level. Lines of arrested growth (LAGs) and wide, strongly birefringent annuli occur throughout the cortex (Figure 4C, F).

The peripheral cortex of the indeterminate cetotheriine rib displays three to four strata separated by annuli and LAGs (Figure 4C), with the lowest stratum consisting of laminar

116 tissue, the central one of woven-parallel bone containing mostly longitudinal osteons and a
117 reversal line (Figure 4E), and the outer one of plexiform bone. This situation suggests
118 differences in sub-periosteal apposition rate during the three growth cycles [13,14]. By
119 contrast, the medial side of the rib displays only longitudinal primary and secondary osteons
120 (Figure 4B).

121 In *Pachyacanthus* and the cetotheriine *Brandtocetus* (Figure 4F), tightening of the LAGs in
122 the outermost cortex gives rise to an external fundamental system (EFS). In *Brandtocetus*, the
123 outermost layer is a thick formation of parallel-fibered tissue with sharp LAGs that is
124 separated from the subjacent woven-parallel tissue by a reversal line (Figure 4F). Both here
125 and in the second, indeterminate cetotheriine, this line could reflect either superficial
126 remodeling related to bone growth [15], or an episode of skeletal resorption related to
127 weaning or starvation.

128 Unlike in the ribs, the medulla of the delphinidan humerus is partly occluded by remnants of
129 calcified cartilage matrix taking the form of amorphous, vitreous tissue covered with thick
130 deposits of endosteal lamellar bone (Figure 4G). Globuli ossei – roundish excrescences
131 protruding from the endosteal deposits into the cartilage matrix, from which they are
132 separated by a sharp, crenellated line – occur throughout the medullary region (Figure 4G
133 insert).

134 Globuli ossei normally occur just below the growth plates, at a level where the conjunctivo-
135 vascular invasion front resorbs the calcified cartilage [16]. During growth, their fate is to be
136 resorbed, remodeled, and ultimately replaced by secondary trabeculae made of endosteal
137 lamellar tissue. Their persistence in the delphinidan humerus means that the normal trajectory
138 of endochondral ossification was shortened: the resorption of the calcified cartilage matrix
139 stopped at an early stage and was locally replaced by protracted endosteal deposition, which

led to the quasi-complete occlusion of the erosion bays initially excavated in the cartilage. Subsequent Haversian re-modeling was weak, but present.

The cortex of the humerus (Figure 4H, insert) is made of a woven-parallel complex in which primary osteons display different orientations depending on the sectional level: in the middle of the shaft, canals are predominantly longitudinal and, to a lesser extent, reticular; towards the distal epiphysis, vascular orientation becomes oblique or radial.

DISCUSSION AND CONCLUSIONS

Prevalence and development of pachyosteosclerosis

Paratethyan baleen whales, dolphins and seals show marked osteosclerosis in the form of compact bones lacking a medullary cavity. Outside the Paratethys, similar patterns only occur in some stem cetaceans (e.g., *Basilosaurus*, Cg ≤ 95.2% [3]) and the – likely benthic – phocids *Nanophoca vitulinoides* (Cg = 99.4%) and *Phocanella pumila* (Cg = 99.7%) from the late middle Miocene to early Pliocene of the North Sea (Table S4) [10, 17]. However, in these environments, many contemporaneous relatives have no pachyosteosclerotic long bones, suggesting against an environmental impact on the development of pachyosteosclerosis in *Basilosaurus, Nanophoca* and *Phocanella*. Comparisons with *Nanophoca* show that osteosclerosis can affect almost the entire postcranial skeleton [10], and thus was plausibly more pronounced in Paratethyan seals than revealed by our limited dataset.

Strongly swollen bones occur throughout the skeleton of both *Pachyacanthus* and cetotheriine baleen whales [18,19] (Figure 2). The extent of pachyostosis in these species is remarkable, with similar levels having only been reported from ‘limbed snakes’ like *Pachyophis woodwardioi* from the Cenomanian of Europe and North Africa [20].

The development of osteosclerosis in Paratethyan marine mammals was driven by two distinct mechanisms: imbalanced remodeling and inhibited resorption of primary trabeculae. During imbalanced remodeling, the amount of secondarily deposited bone surpasses the quantity of resorbed primary tissue. This process is widespread among aquatic amniotes [21-23] and evident in all of our seals, *Pachyacanthus* and the two cetotheriines, as well as *Nanophoca* from the Neogene of the North Sea Basin [10].

Inhibited resorption of primary trabeculae combined with an increase in intertrabecular deposits occurs in the delphinidan humerus, as well as sirenians [24], basilosaurid stem cetaceans [2], and several aquatic reptiles [25-27]. The two mechanisms are not mutually exclusive. As shown by the delphinidan humerus, typical Haversian remodeling can contribute to a compaction process initiated through inhibited resorption.

Evolutionary drivers

Pachyosteosclerosis in stem cetaceans likely assisted with passive buoyancy control and trim regulation [28-30], but this hydrostatic solution was ultimately supplanted by more sophisticated hydrodynamic structures and behaviors [28, 30-32] including, among others, a global decrease in skeletal mass and volume [33]. The presence of (pachy)osteosclerosis in Paratethyan marine mammals is thus both convergent, given its widespread taxonomic distribution and disparate underlying developmental mechanisms, and seemingly a reversal towards an ancient adaptation.

Osteosclerosis is absent in extant marine mammals, except in juvenile bowhead whales (*Balaena mysticetus*). Ribs in this species are initially amedullary and highly compact, but then assume a more normal tubular architecture as calcium and phosphates are remobilized for the preferential growth of the massive head [34]. Similar growth patterns are common

among mammals, but cannot explain our Paratethyan fossils for several reasons. First, osteosclerosis in their case clearly persists into adulthood [18,20,35]. Secondly, none of our specimens show significant porosity that could indicate episodes of sustained bone resorption. Finally, the sheer degree of osteosclerosis would likely have demanded attendant behavioral adaptations (e.g., with regards to buoyancy, swimming speed and maneuverability), and as such was likely not just a transitory feature.

Besides mineral recycling, dense bones may also serve as ballast to counteract the effects of hypersalinity, which increases sea water density and thus, buoyancy [36]. Indeed, (pachy)osteosclerosis only became prominent in the Central Paratethys after falling sea levels around 13.8 Ma turned most of its basins hypersaline (Figure S1) [5,37]. This 'Badenian Salinity Crisis' (BSC) ceased with the opening of a strong connection with the brackish Eastern Paratethys (Figures 1, S1)[9,37], and was followed by an eastward dispersal of whales, dolphins and seals around 12.65 Ma (Figure 1)[7].

Given its largely coeval, convergent and geographically restricted emergence among three marine mammal clades, (pachy)osteosclerosis could plausibly have evolved as a regional adaptation to hypersalinity before spreading east across the entire Paratethys. Why pachyosteosclerosis persisted in the normal salinity or even brackish conditions that followed the BSC remains unclear, but could perhaps be explained by dense bones acting as an exaptation for benthic foraging, as has been proposed for cetotheriids in particular [38].

The Paratethys was an inland sea whose hydrological, chemical and physical characteristics were profoundly affected by even minor tectonic and climatic changes [8,9,37]. Future sea level rises may form shallow seas or connect currently isolated water masses. Similar to the Miocene Paratethys, minor geographic changes will have a profound impact on these environments and may create ecological niches for marine mammals not unlike those of the ancient Paratethys.

ACKNOWLEDGEMENTS

We thank Gerhard Wanzenböck, Ursula Göhlich from the Naturhistorisches Museum Wien (Vienna, Austria), and Oleksandr Kovalchuk from the National Museum of Natural History of the National Academy of Sciences of Ukraine (Kiev, Ukraine) for proving access to specimens; S. Bruaux, C. Cousin, A. Folie and O. Pauwels from the Institut royal des Sciences naturelles de Belgique (Brussels, Belgium), C. de Muizon from the Muséum national d'Histoire naturelle (Paris, France), and D.J. Bohaska, M.R. McGowen, and N.D. Pyenson from the Smithsonian National Museum of Natural History (Washington, D.C., U.S.) for providing access to comparison material.

Financial: LD in part funded by the Society of Vertebrate Paleontology's Stephen Cohen Award for this project and other projects on inner bone structure of Phocidae and by the Fonds National de la Recherche Scientifique, chargé de recherche grant 34788495. PG in part funded by the National Research Foundation of Ukraine, grant 2020.02/0247.

REFERENCES

1. Buffrénil, V. de, Canoville, A., D'Anastasio, R., and Domning, D.P. (2010). Evolution of sirenian pachyosteosclerosis, a model-case for the study of bone structure in aquatic tetrapods. J. Mamm. Evol. *17*, 101-120.

2. Buffrénil, V. de, Ricqlès, A. de, Ray, C. E., and Domning, D. P. (1990). Bone histology of the ribs of the archaeocetes (Mammalia: Cetacea). J. Vertebr. Paleontol. *10*, 455-466.

3. Houssaye, A., Tafforeau, P., Muizon, C. de, and Gingerich, P. D. (2015). Transition of Eocene whales from land to sea: evidence from bone microstructure. Plos One *10*, e0118409.

4. Buffrénil, V. de, and Schoevaert, D. (1988). On how the periosteal bone of the delphinid humerus becomes cancellous: ontogeny of a histological specialization. J. Morphol. *198*, 149-164.

5. Simon, D., Palcu, D., Meijer, P., and Krijgsman, W. (2018). The sensitivity of middle Miocene paleoenvironments to changing marine gateways in Central Europe. Geology *47*, 35-38.

6. Gol'din, P., and Startsev, D. (2017). A systematic review of cetothere baleen whales (Cetacea, Cetotheriidae) from the Late Miocene of Crimea and Caucasus, with a new genus. Pap. Palaeontol. *3*, 49-68.

7. Gol'din, P., Haiduc, B. S., Kovalchuk, O., Gorka, M., Otryazhyi, P., Branzila, M., Paun, E. I., Barkaszi, Z., Tibuleac, P., and Ratoi, B. G. (2020). The Volhynian (late Middle Miocene) marine fishes and mammals as proxies for the onset of the Eastern Paratethys re-colonisation by vertebrate fauna. Palaeontol. Electron. *23*, a43.

8. Palcu, D.V., Tulbure, M., Bartol, M., Kouwenhoven, T.J., and Krijgsman, W. (2015). The Badenian–Sarmatian Extinction Event in the Carpathian foredeep basin of Romania: Paleogeographic changes in the Paratethys domain. Global Planet. Change *133*, 346-358.

9. Palcu, D.V., Golovina, L.A., Vernyhorova, Y.V., Popov, S.V., and Krijgsman, W. (2017). Middle Miocene paleoenvironmental crises in Central Eurasia caused by changes in marine gateway configuration. Global Planet. Change *158*, 57-71.

10. Dewaele, L., Lambert, O., Laurin, M., De Kock, T., Louwye, S., and Buffrénil, V. de. (2019). Generalized osteosclerotic condition in the skeleton of *Nanophoca vitulinoides*, a dwarf seal from the Miocene of Belgium. J. Mamm. Evol. *26*, 517-543.

11. Girondot, M., and Laurin, M. (2003). Bone Profiler: a tool to quantify, model, and statistically compare bone section compactness profiles. J. Vertebr. Paleontol. *23*, 458-461.

12. Nakajima, Y., and Endo, H. (2013). Comparative microanatomy of terrestrial, semiaquatic and aquatic carnivorans using micro-focus CT Scan. Mamm. Study *38*, 1-8.

13. Amprino, R. (1947). La structure du tissu osseux envisagée comme expression de différences dans la vitesse de l'accroissement. Arch. Biol. *58*, 315-330.

14. Castanet, J., Curry Rogers, C., Cubo, J., and Boisard, J. (2000). Periosteal bone growth rates in extant ratites (ostrich and emu). Implications for assessing growth in dinosaurs. C.R. Acad. Sci. Paris Sci. Vie *323*, 543-550.

15. Enlow, D.H. (1693). *Principles of bone remodeling*. Springfield, Ill, Ch. C. Thomas.

16.Quilhac, A., Zylbergerg, L., and Ricqlès, A. de (2014). Globuli ossei in the long bones of *Pleurodeles waltl* (Amphibia, Urodela, Salamandridae). J. Morphol. *275*, 1226-1237.

17. Dewaele, L., Amson, E., Lambert, O., and Louwye, S. (2017). Reappraisal of the extinct seal "*Phoca*" *vitulinoides* from the Neogene of the North Sea basin, with bearing on its geological age, phylogenetic affinities, and locomotion. PeerJ *5*, e3316.

18. Kazár, E. (2010). Revision of the genus *Pachyacanthus* Brandt, 1971 (Mammalia: Cetacea: Odontoceti). Ann. Naturhist. Mus. Wien, ser. *112*, 537-568.

19. Gol'din, P., Startsev, D., and Krakhmalnaya, T. (2014). The anatomy of the Late Miocene baleen whale *Cetotherium riabinini* from Ukraine. Acta Palaeontol. Pol. *59*, 795-815.

20. Houssaye, A. (2013). Palaeoecological and morphofunctional interpretation of bone mass increase: an example in late cretaceous shallow marine squamates. Biol. Rev *88*, 117-139.

21. Buffrénil, V. de, and Mazin, J.-M. (1989). Bone histology of *Claudiosaurus germaini* (Reptilia, Claudiosauridae) and the problem of pachyostosis in aquatic tetrapods. Hist. Biol. *2*, 311-322.

22. Lambert, O., Muizon, C. de, and Buffrénil, V. de. (2011). Rostral densification in beaked whales: diverse processes for a similar pattern. C. R. Palevol *10*, 453-468.

23. Amson, E., Muizon, C. de, Laurin, M., Argot, C., and Buffrénil, V. de. (2014). First evidence of gradual adaptation of bone structure to aquatic lifestyle in fossil sloths. P. Roy. Soc. B-Biol. Sci. *281*, 1-6.

24. Buffrénil, V. de, and Schoevaert, D. (1989). Données quantitatives et observations histologiques sur la pachyostose du squelette du dugong, *Dugong dugon* (Müller) (Sirenia, Dugongidae). Can. J. Zool. *67*, 2107-2119.

25. Ricqlès, A. de. (1976). On bone histology of fossil and living reptiles, with comments on its functional and evolutionary significance. In Morphology and biology of Reptiles, A. d'A. Bellairs, and C. Barry Cox, eds. (Lin. Soc. Symp. Ser. N°3), pp. 123-151.

26. Ricqlès, A. de, and Buffrénil, V. de. (2001). Bone histology, heterochronies and the return of tetrapods to life in water: w[h]ere are we? In Secondary Adaptation of Tetrapods to life in Water, J-M. Mazin, and V. de Buffrénil, eds. (München: Verlag Dr. Friedrich Pfeil), pp. 289-310.

27. Houssaye, A. (2009). Pachyostosis in aquatic amniotes: a review. Integr. Biol. *4*, 325-340.

28. Fish, F.E. (1993). Influence of hydrodynamic design and propulsion mode on mammalian swimming energetics. Aust. J. Zool. *42*, 79-101.

29. Taylor, M.A. (2000). Functional significance of bone ballast in the evolution of buoyancy control strategies by aquatic tetrapods. Hist. Biol. *14*, 15-31.

30. Gray, N.-M., Kainec, K., Madar, S., Tomko, L., and Wolfe, S. (2007). Sink or swim? Bone density as a mechanism for buoyancy control in early cetaceans. Anat. Rec. *290*, 638-653.

31. Williams, T.M. (2009). Swimming. In Encyclopaedia of marine mammals, W.F. Perrin, B. Würsig, and J.G.M. Thewissen, eds. (Amsterdam: Academic Press (Elsevier)), pp. 1140-1147.

32. Houssaye, A., Sander, P. M., and Klein, N. (2016). Adaptive patterns in aquatic amniote bone microanatomy – More complex than previously thought. Integr. Comp. Biol. *56*, 1-21.

33. Webb, P. and Buffrénil, V. de (1990). Locomotion in the biology of large aquatic vertebrates. Trans. Am. Fish Soc. *119*, 629-641.

34. George, J. C., Stimmelmayr, R., Suydam, R., Usip, S., Givens, G., Sformo, T., and Thewissen, J. G. M. (2016). Severe bone loss as part of the life history strategy of bowhead whales. PloS One *11*, e0156753.

35. Gol'din, P. (2018). New Paratethyan dwarf baleen whales mark the origin of cetotheres. PeerJ *6*, e5800.

36. Piñeiro, G., Ramos, A., Goso, C., Scarabino, F., and Laurin, M. (2012). Unusual Environmental Conditions Preserve a Permian Mesosaur-Bearing Konservat-Lagerstätte from Uruguay. Acta Palaeontol. Pol. *57*, 299-318.

37. Palcu D.V., Patina, I.S., Sandric, I., Lazarev, S., Vasiliev, I., Stoica, M., and Krijgsman, W. (2021). Late Miocene megalake regression in Eurasia. Sci. Rep. *11*, 11471.

323 38. Gol'din, P., Startsev, D., and Krakhmalnaya, T. (2014). The anatomy of the Late Miocene
324 baleen whale *Cetotherium riabinini* from Ukraine. Acta Palaeontol. Pol. *59*, 795-814.

325 39. Koretsky, I.A. (2001). Morphology and systematics of the Miocene Phocinae (Mammalia:
326 Carnivora) from Paratethys and the North Atlantic region. Geol. Hun. Ser. Palaeontol. *54*,
327 1-109.

328 40. Koretsky, I.A., and Grigorescu, D. (2002). The fossil monk seal *Pontophoca sarmatica*
329 (Alekseev) (Mammalia: Phocidae: Monachinae) from the Miocene of eastern Europe. Sm.
330 C. Paleob. *93*, 149-162.

331 41. Koretsky, I.A., and Rahmat, S.J. (2013). First record of fossil Cystophorinae (Carnivora,
332 Phocidae): middle Miocene seals from the northern Paratethys. Riv. Ital. Paleontol. S. *119*,
333 335-350.

334 42. Pia, J. (1936). Von der Walen des Wiener Miozäns. Mitt. Österr. Geol. G. *29*, 357-428.

335 43. Francillon-Vieillot H., Buffrénil, V. de, Castanet, J., Géraudie, J., Meunier, F.J., Sire, J.-
336 Y., Zylberberg, L., and Ricqlès, A. de. (1990). Microstructure and mineralization of
337 vertebrate skeletal tissues. In Skeletal Biomineralization: Patterns, Processes and
338 Evolutionary Trends, Vol. 1, J.G. Carter, ed. (New York, Van Nostrand Reinhold), pp.
339 471-530.

340 44. Prondvai, E., Stein, K.H.W., Ricqlès, A. de, and Cubo, J. (2014). Development-based
341 rivision of bone tissue classification: the importance of semantics for science. Biol. J. Linn.
342 Soc. *112*, 799-816.

343 45. Lamm, E.T. (2013). Preparation and sectioning of specimens. In Bone Histology of Fossil
344 Tetrapods: Advancing Methods, Analysis, and Interpretation, K. Padian, and E.T. Lamm,
345 eds. (Berkeley: University of California Press), pp 55–160

MAIN-TEXT FIGURE LEGENDS

Figure 1. Paleogeographic, paleoceanographic and temporal overview. (A) Simplified paleogeographic map of the Central and Eastern Paratethys during the middle Serravallian, (ca. 13 Ma), with specimen localities indicated (see Figure S1 and Table S1 for details). Map adapted from Palcu et al. (2015)[8]. (B) Simplified paleogeographic and paleoceanographic map of the Paratethys during the early Serravallian Badenian Salinity Crisis (BSC) (ca. 13.8-13.4 Ma), showing the endorheic conditions that created the hypersaline conditions in the Central Paratethys. Arrows indicate flow direction. Map adapted from Palcu et al. (2017)[9] (see Figure S1 for more details). (C) Temporal ranges of the specimens for the different taxa in this study, showing that all specimens post-date the BSC. After the BSC, these clades dispersed throughout the Central and Eastern Paratethys: specimens are geologically younger towards the East (A, C). The independent development of pachyosteosclerosis in seals, toothed whales and baleen whales (inferred from the fact that their closest known relatives, not shown here, lack pachyosteosclerosis) originated in hypersaline conditions in the Central Paratethys, during the BSC.

Figure 2. Osteosclerosis affecting the ribs and limb bones of Miocene marine mammals from the Paratethys. (A) Lumbar vertebra of cf. Platanistidae *Pachyacanthus suessii*, from the late Serravallian of the Vienna Basin, Austria, in posterior (left) and left lateral (right) views, showing the marked swelling of the neural spine and, to a lesser extent, transverse processes. (B) Rib of the cetotheriine mysticete *Brandtocetus chongulek*. (C) Rib of the platanistid dolphin *Pachyacanthus suessi*. (D) Rib of an indeterminate cetotheriine. (E) cross sections through the diaphysis (E1) and distal metaphysis (E2) of the humerus of an

indeterminate delphinidan. (F, G) Location of the reference ("mid diaphyseal") cross sections sampled in the limb bones of the Paratethyan seals. The humerus of *Monachopsis pontica* (F) and the femur of *Praepusa* sp. (G), both in frontal and lateral views are taken as examples. (H) Section in the humerus of *Pachyphoca chapskii*. (I) Humerus of *Monachopsis pontica*. (J) Humerus of *Cryptophoca maeotica*. (K) Humerus of "*Phoca*" *bessarabica*. (L) Femur of *Pontophoca sarmatica*. (M) Femur of *Praepusa* sp. (N) Humerus of *Sarmatonectes sintsovi*. Thin sections in ordinary transmitted light.

Figure 3. Histological features of Miocene seal limb bones from the Paratethys. (A) Remodeled compacted spongiosa in the medullary region of the humerus of *Monachopsis pontica* (polarized light). (B) Dense Haversian remodeling in the deep humeral cortex of *M. pontica* (polarized light). (C) Woven-parallel complexes in the primary periosteal cortex of the humerus of *Sarmatonectes sintsovi*. The deep cortex is made of laminar to plexiform tissue, but the primary osteons become longitudinal in more peripheral layers. Asterisks denote conspicuous birefringent *annuli* (right, ordinary transmitted light; left, polarized light). (D) Periosteal cortex of the femur of *Praepusa* sp. (E) Femoral cortex of *Pontophoca sarmatica*. (F) Humeral cortex of *Pachyphoca chapskii* with diffuse annuli. The features of the specimens (D-F) resemble those of *S. sintsovi*. (G) Conspicuous annuli of birefringent parallel-fibered tissue in the peripheral cortex of *Cryptophoca maeotica*. (H) Conspicuous lines of arrested growth on a background of parallel-fibered tissue in the peripheral cortex of the *Monachopsis* humerus.

Figure 4. Histology of Miocene cetacean bones from the Paratethys. (A) Densely remodeled tissue in the rib of the cetotheriine mysticete *Brandtocetus*. (B) Woven-parallel

complex with longitudinal primary osteons and sustained Haversian remodeling in the medial cortex of an indeterminate cetotheriine rib. (C) Variation of the tissue types in the periosteal cortex of the cetotheriine rib. (D) Laminar bone tissue in the peripheral cortex of the platanistid dolphin *Pachyacanthus*. (E) Characteristic resorption line (asterisk) in the middle of the cortex of the cetotheriine rib. (F) Annuli and lines of arrested growth in the peripheral cortex of the *Brandtocetus* rib. The outer cortex is limited to the depth by a reversion line (asterisk). (G) Remnants of calcified cartilage matrix (cc) and globuli ossei in the medulla of the delphinidan humerus. (H) Woven-parallel complex with longitudinal primary osteons in the deep primary cortex of the delphinidan humerus. There are signs of mild Haversian remodeling (polarized light). Insert shows a more peripheral region of the cortex with almost no evidence of Haversian remodeling. The primary bone deposit is of a loose reticular type.

STAR METHODS

CONTACT FOR REAGENT AND RESOURCE SHARING

Further information and requests for resources and reagents should be directed to and will be fulfilled by the Lead Contact, Leonard Dewaele (ldewaele@uliege.be).

KEY RESOURCE TABLE

Reagent or resource	Source	Identifier
Deposited data		

Osteohistological slides	This paper	Histothèque of the Muséum national d'Histoire naturelle (Paris, France)
Software and algorithms		
Bone Profiler Version 4.5.8.	[11]	This version of the software is no longer available online, but a more recent version can be downloaded at: http://134.158.74.46/BoneProfileR/
Prism	Graphpad	https://www.graphpad.com/scientific-software/prism/

METHOD DETAILS

Taxonomic sample

We studied bone dimensions, compactness and osteohistology in seven true seals (phocids), two baleen whales (mysticetes), and two toothed whales (odontocetes) from the middle to late Miocene of the Paratethys (Tables S1–S5).

The evolutionary affinities of the sampled seals remain controversial, but they include one putative monachine (*Pontophoca sarmatica*), four possible phocines (*Cryptophoca maeotica*, *Monachopsis pontica*, *Praepusa* sp., and *Sarmatonectes sintsovi*), and two species of uncertain subfamilial affinities ('*Phoca*' *bessarabica* and *Pachyphoca chapskii)* [39-41]. Both of the mysticetes (*Brandtocetus chongulek* and one indeterminate specimen) represent cetotheriines, a diverse clade of relatively small baleen whales that appear endemic to the Paratethys and generally date to the latest Serravallian or early Tortonian [6]. Finally, the odontocetes (toothed whales) include one undetermined delphinidan and the putative platanistid *Pachyacanthus suessi* [18,42].

Samples were taken from well-preserved humeri, femora or partial ribs with no obvious signs of crushing or epigenisation. For context, we also collected comparative data on a variety of other extant and extinct marine mammals based on first-hand observations and the literature (Tables S1–S5).

Sampling and measurement protocols

We assessed the presence and underlying mechanisms of pachyosteosclerosis in our samples via a combination of gross anatomy, microanatomy, and histology.

Gross anatomy

Pachyostosis (i.e. cortical thickening) of the seal long bones was quantified via the 'bulkiness index' (BI) of Dewaele et al. (2018)[10], which considers the maximum proximodistal length (BL); transverse width at mid-shaft (TW); and anteroposterior width (APW), measured perpendicular to and at the same level as TW (Figure S3).

For the humerus:

$$BI = TW/BL$$

Whereas for the femur:

$$BI = [0.5*(TW+APW)]/BL.$$

In both cases, high values indicate a relatively thick (i.e. pachyostotic) shaft.

Microanatomy

Microanatomical studies were conducted with Bone Profiler Version 4.5.8., which models the distribution of osseous tissue from the center towards the periphery of a section through a sigmoid curve with four parameters: S, P, Min, and Max [11].

S = reciprocal of the slope at the curve inflection point; it is proportional to the relative width of the transition zone between the medulla and the cortical regions;

P = position of the curve inflection point on the x axis and represents the position of the transition area between the medulla and the cortical region;

Min and Max = minimum and maximum asymptotes, respectively, representing the minimum and maximum values of bone compactness in a section, typically in the central medulla and peripheral cortex, respectively.

In addition, Bone Profiler calculates global compactness (Cg), which is the area of a section (in %) occupied by bone tissue. Statistical calculations were made with the software Prism (GraphPad ed.). Microanatomical and histological terminology follows Francillon-Vieillot et al. (1990) and Prondvai et al. (2014) [43,44].

Osteohistology

Thin sections of all bones were produced following Lamm (2013)[45], and have been accessioned into the Histothèque of the Muséum national d'Histoire naturelle (Paris, France) (Table S5). Ground sections were 80–100 µm thick and examined at low (x 10) and medium

(x 400) magnification in transmitted ordinary and polarized light. Because of their incompleteness, we sectioned the cetacean bones orthogonal to their long axis in 2–3 mm intervals. By contrast, the seal bones were sectioned thrice, at a level approximately two thirds the length of the bone measured from the proximal epiphysis (or the humeri), or the distal epiphysis (for the femora). In both cases, the sections aim to coincide with the 'neutral plane', which includes the spot from which ossification of the bone proceeded [12]. Additional sections were made through the proximal two thirds of the humerus of *Cryptophoca maeotica*, *Pachyphoca chapskii*, and '*Phoca*' *bessarabica* (cross sections, spaced 1 cm apart), and the proximal third of each femur, in a longitudinal plane passing through the great trochanter and the middle of the condyle (Figure S2).

Institutional abbreviations

IRSNB, Royal Belgian Institute of Natural Sciences, Brussels, Belgium; **MAB**, Museum "de Groene Poort", Boxtel, Netherlands; **NMNHU**, National Museum of Natural History, National Academy of Sciences of Ukraine, Kiev, Ukraine; **PIN**, Paleontological Institute of the Academy of Sciences of Russia, Moscow, Russia; **USNM**, Smithsonian National Museum of Natural History, Washington, D.C., U.S.

SUPPLEMENTAL ITEM TITLES

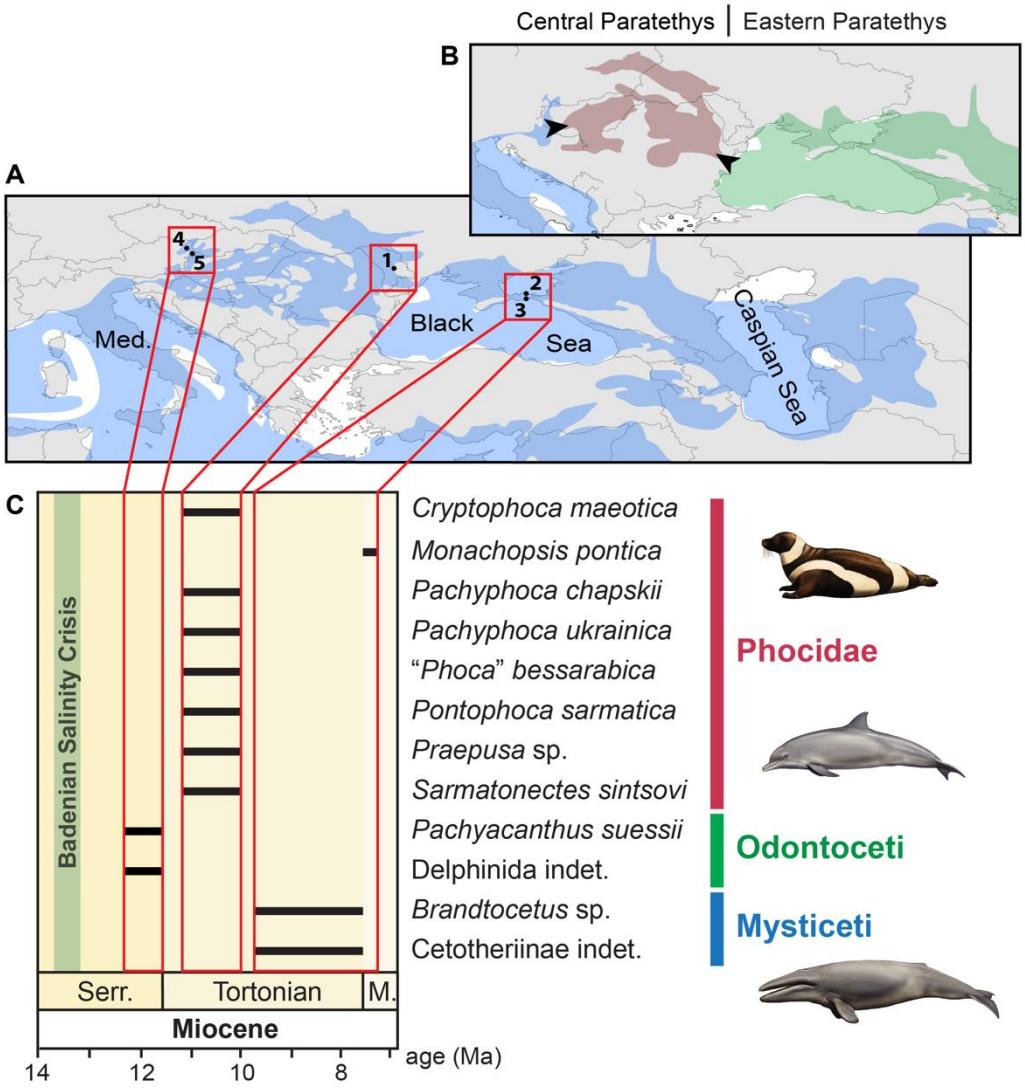

Figure 1. Paleogeographic, paleoceanographic and temporal overview. (A) Simplified paleogeographic map of the Central and Eastern Paratethys during the middle Serravallian, (ca. 13 Ma), with specimen localities indicated (see Figure S1 and Table S1 for details). Map adapted from Palcu et al. (2015)[8]. (B) Simplified paleogeographic and paleoceanographic map of the Paratethys during the early Serravallian Badenian Salinity Crisis (BSC) (ca. 13.8-13.4 Ma), showing the endorheic conditions that created the hypersaline conditions in the Central Paratethys. Arrows indicate flow direction. Map adapted from Palcu et al. (2017)[9] (see Figure S1 for more details). (C) Temporal ranges of the specimens for the different taxa in this study, showing that all specimens post-date the BSC. After the BSC, these clades dispersed throughout the Central and Eastern Paratethys: specimens are geologically younger towards the East (A, C). The independent development of pachyosteosclerosis in seals, toothed whales and baleen whales (inferred from the fact that their closest known relatives, not shown here, lack pachyosteosclerosis) originated in hypersaline conditions in the Central Paratethys, during the BSC.

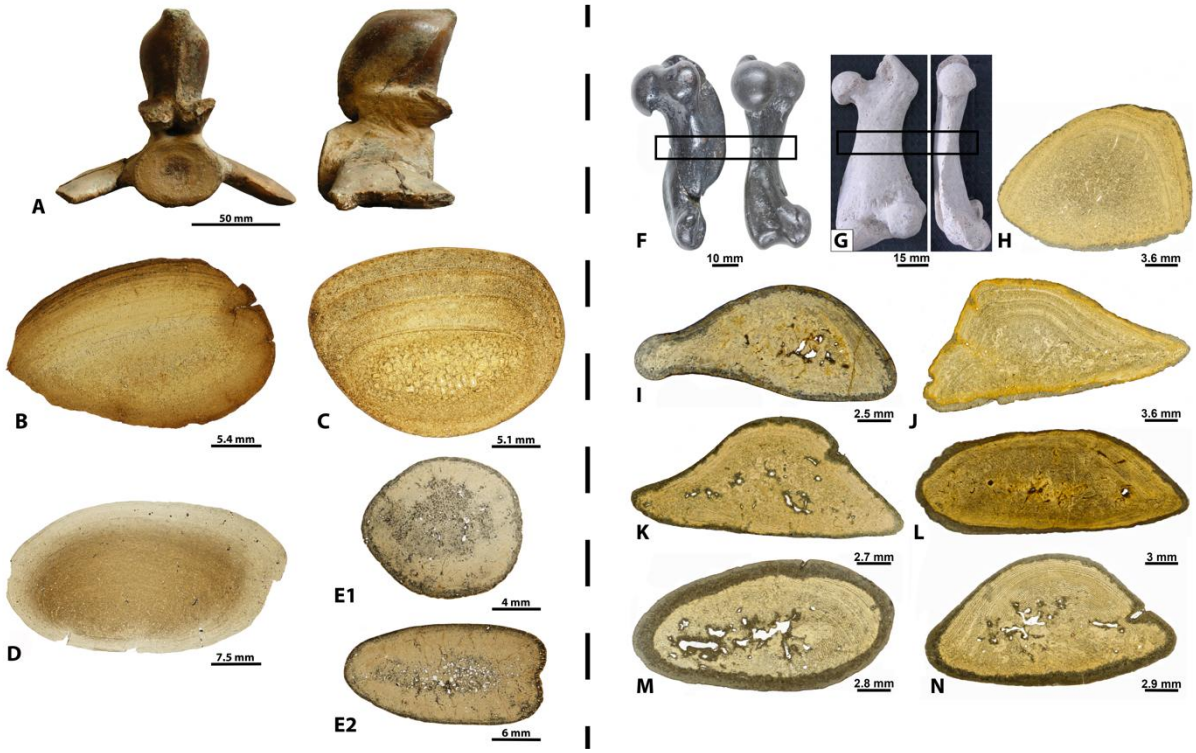

514

515 **Figure 2. Osteosclerosis affecting the ribs and limb bones of Miocene marine mammals**
516 **from the Paratethys.** (A) Lumbar vertebra of cf. Platanistidae *Pachyacanthus suessii*, from
517 the late Serravallian of the Vienna Basin, Austria, in posterior (left) and left lateral (right)
518 views, showing the marked swelling of the neural spine and, to a lesser extent, transverse
519 processes. (B) Rib of the cetotheriine mysticete *Brandtocetus chongulek*. (C) Rib of the
520 platanistid dolphin *Pachyacanthus suessi*. (D) Rib of an indeterminate cetotheriine. (E) cross
521 sections through the diaphysis (E1) and distal metaphysis (E2) of the humerus of an
522 indeterminate delphinidan. (F, G) Location of the reference ("mid diaphyseal") cross sections
523 sampled in the limb bones of the Paratethyan seals. The humerus of *Monachopsis pontica* (F)
524 and the femur of *Praepusa* sp. (G), both in frontal and lateral views are taken as examples.
525 (H) Section in the humerus of *Pachyphoca chapskii*. (I) Humerus of *Monachopsis pontica*. (J)
526 Humerus of *Cryptophoca maeotica*. (K) Humerus of "*Phoca*" *bessarabica*. (L) Femur of
527 *Pontophoca sarmatica*. (M) Femur of *Praepusa* sp. (N) Humerus of *Sarmatonectes sintsovi*.
528 Thin sections in ordinary transmitted light.

529

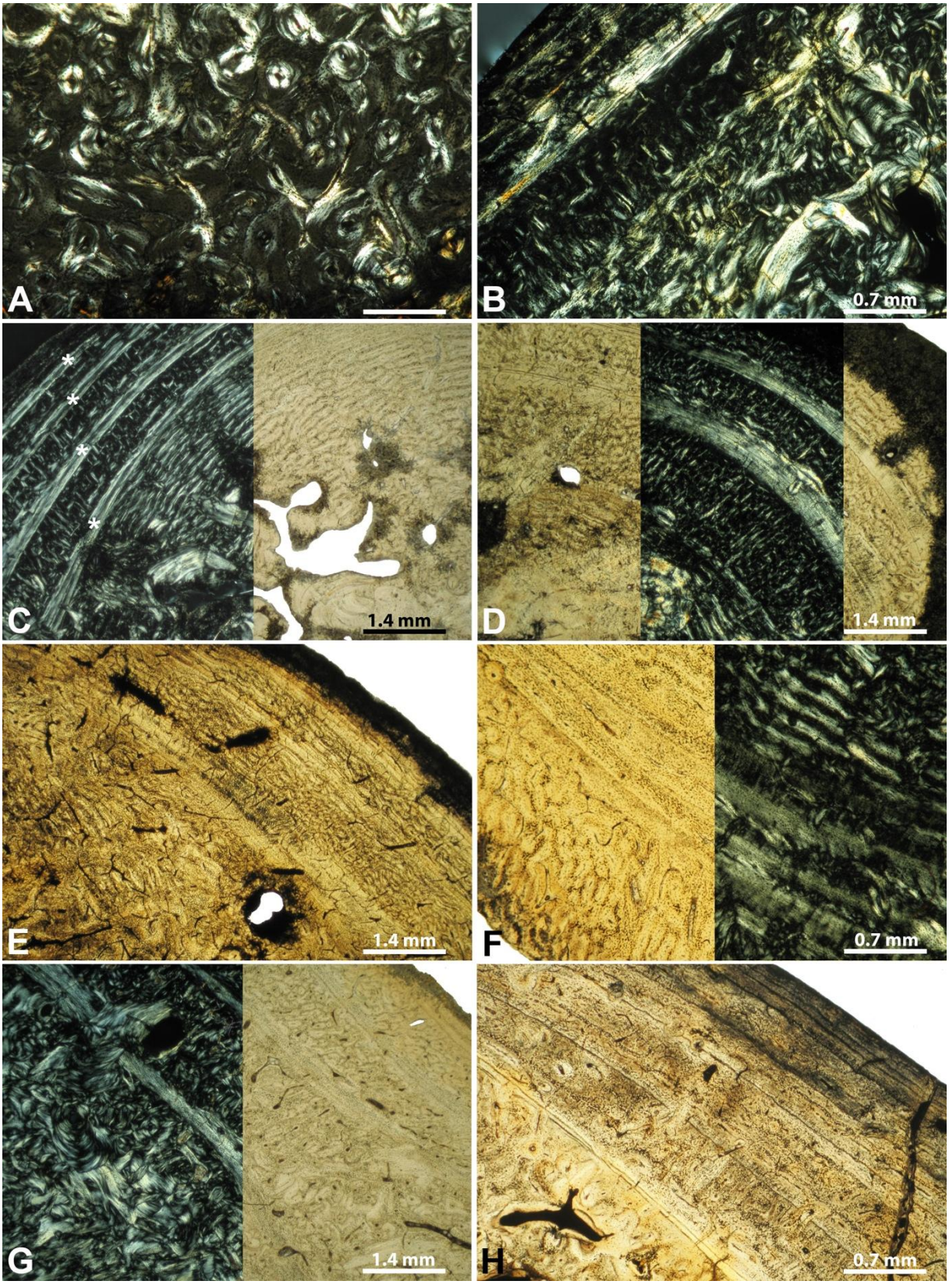

Figure 3. Histological features of Miocene seal limb bones from the Paratethys. (A) Remodeled compacted spongiosa in the medullary region of the humerus of *Monachopsis pontica* (polarized light). (B) Dense Haversian remodeling in the deep humeral cortex of *M. pontica* (polarized light). (C) Woven-parallel complexes in the primary periosteal cortex of

the humerus of *Sarmatonectes sintsovi*. The deep cortex is made of laminar to plexiform tissue, but the primary osteons become longitudinal in more peripheral layers. Asterisks denote conspicuous birefringent *annuli* (right, ordinary transmitted light; left, polarized light). (D) Periosteal cortex of the femur of *Praepusa* sp. (E) Femoral cortex of *Pontophoca sarmatica*. (F) Humeral cortex of *Pachyphoca chapskii* with diffuse annuli. The features of the specimens (D-F) resemble those of *S. sintsovi*. (G) Conspicuous annuli of birefringent parallel-fibered tissue in the peripheral cortex of *Cryptophoca maeotica*. (H) Conspicuous lines of arrested growth on a background of parallel-fibered tissue in the peripheral cortex of the *Monachopsis* humerus.

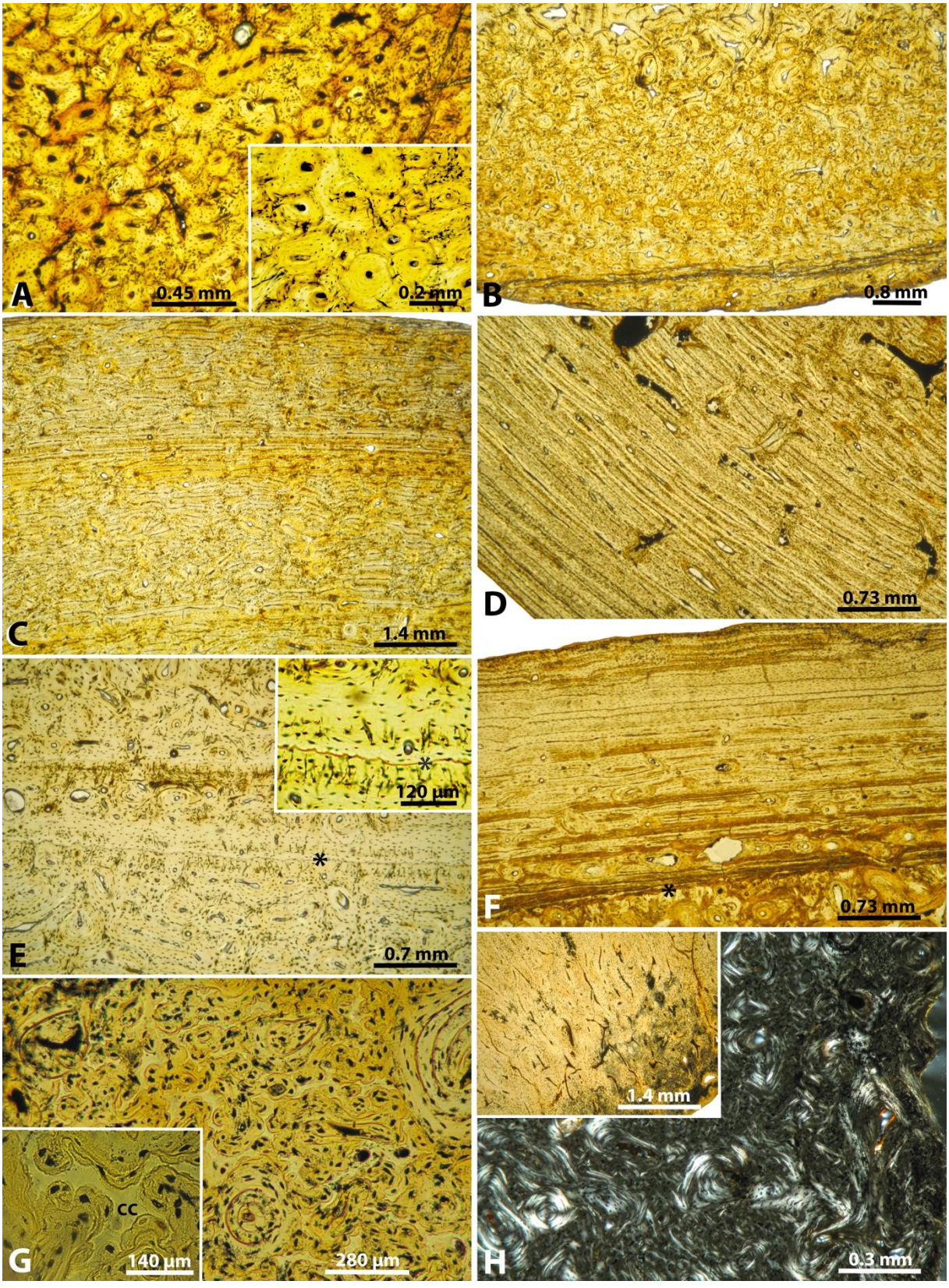

Figure 4. Histology of Miocene cetacean bones from the Paratethys. (A) Densely remodeled tissue in the rib of the cetotheriine mysticete *Brandtocetus*. (B) Woven-parallel complex with longitudinal primary osteons and sustained Haversian remodeling in the medial cortex of an indeterminate cetotheriine rib. (C) Variation of the tissue types in the periosteal

cortex of the cetotheriine rib. (D) Laminar bone tissue in the peripheral cortex of the platanistid dolphin *Pachyacanthus*. (E) Characteristic resorption line (asterisk) in the middle of the cortex of the cetotheriine rib. (F) Annuli and lines of arrested growth in the peripheral cortex of the *Brandtocetus* rib. The outer cortex is limited to the depth by a reversion line (asterisk). (G) Remnants of calcified cartilage matrix (cc) and globuli ossei in the medulla of the delphinidan humerus. (H) Woven-parallel complex with longitudinal primary osteons in the deep primary cortex of the delphinidan humerus. There are signs of mild Haversian remodeling (polarized light). Insert shows a more peripheral region of the cortex with almost no evidence of Haversian remodeling. The primary bone deposit is of a loose reticular type.

SUPPLEMENTARY FIGURES AND TABLES

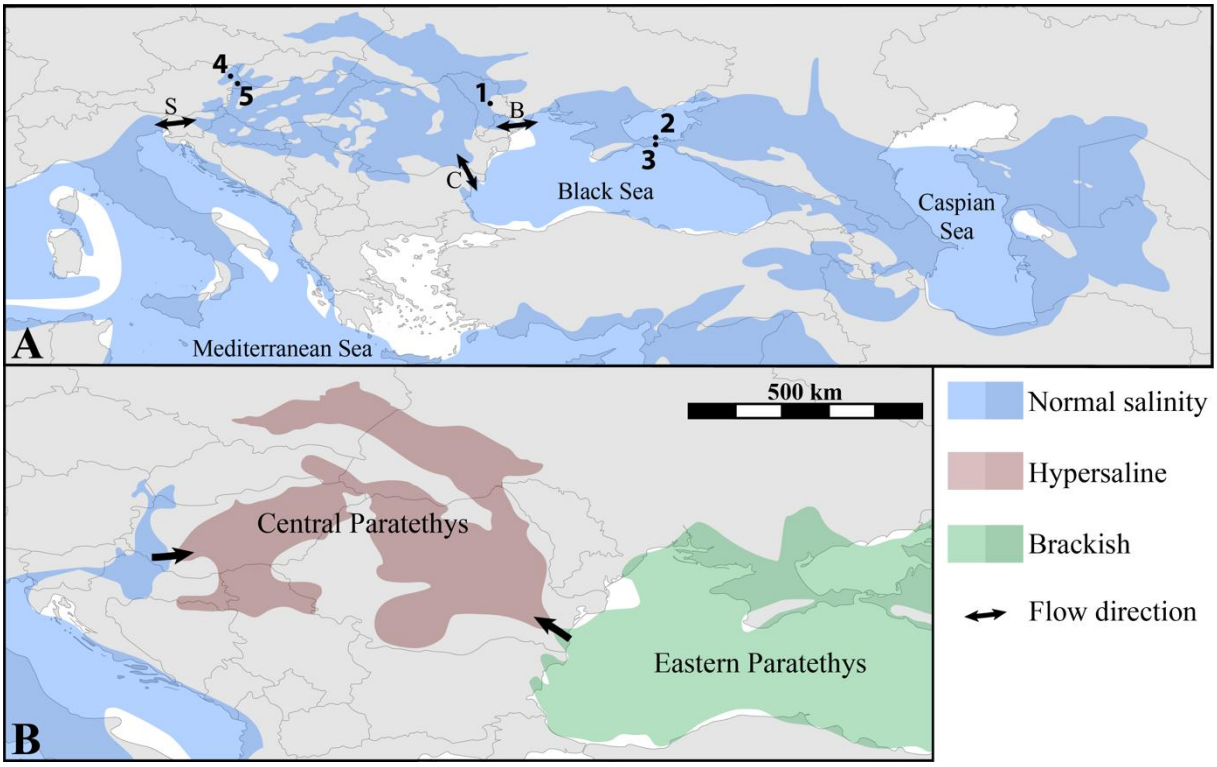

Figure S1. Paleogeography of the Central and Eastern Paratethys during the Neogene. (A) Extent of the Paratethys during the middle Serravallian, around the Badenian-Sarmatian boundary (ca. 13 Ma), following the Badenian Salinity Crisis (BSC). Map adapted from Palcu et al. (2015)[S1]. Specimen localities are indicated (see Table S1 for details). Locality data: 1) Hulbocica (Chisinau, Moldova); middle to upper Bessarabian (Tortonian, late Miocene [S2]. 2) Khroni Cape north of Osovini, Kerch peninsula (Crimea, Ukraine); uppermost Chersonian (Tortonian, late Miocene) [S3-5]. 3) South coast of Tobechick Lake, Kerch Peninsula (Crimea, Ukraine); Chersonian (Tortonian, late Miocene). 4) Nussdorf-Heiligenstadt/ Hernals, (Vienna, Austria); Sarmatian (Serravallian, late middle Miocene) [S6,7]. 5) Bruckneudorf (Burgenland, Austria); Sarmatian (Serravallian, late middle Miocene) [S8]. Arrows indicate sea water flows through important straits, i.e., **B**, Barlad Strait, **C**, Carasu Strait, and **S**, Slovenian Strait. (B) Paratethys during the early Serravallian BSC (ca. 13.8-13.4 Ma),

showing the endorheic conditions that led to the hypersaline conditions in the Central Paratethys. Map adapted from Palcu et al. (2017)[S9].

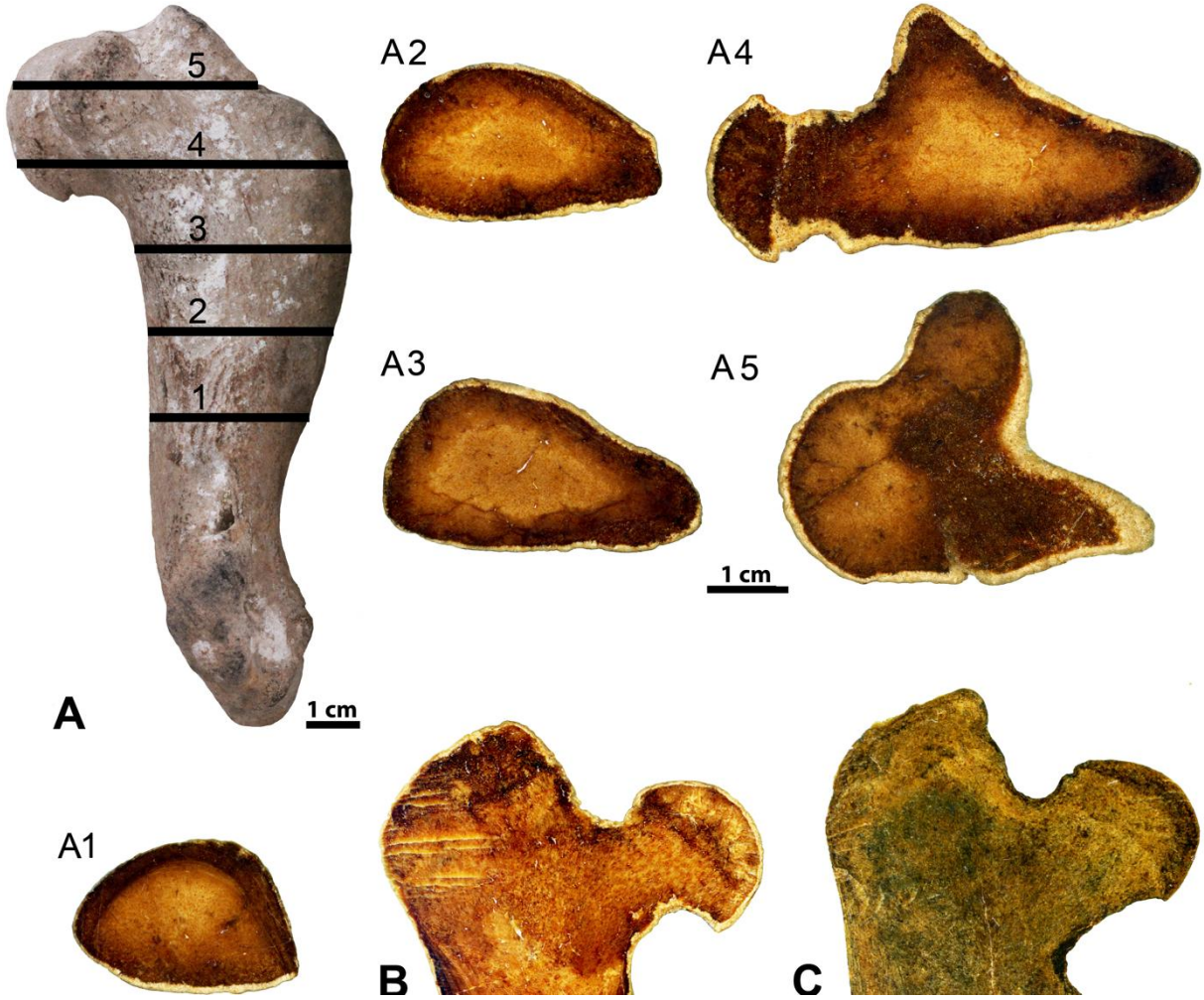

Figure S2. Bone compactness in metaphyses and epiphyses. Additional cross sections made in the metaphyseal and epiphyseal regions of the seal bones. (A) Cross-sections of the humerus of *Pachyphoca chapskii*. All sections in this bone, whatever their level show an extremely high compactness and the absence of any important cavities. (B) Coronal section in the proximal head of the femur in *Sarmatonectes sintsovi*. (C) Coronal section in the femur of *Pachyphoca ukrainica*.

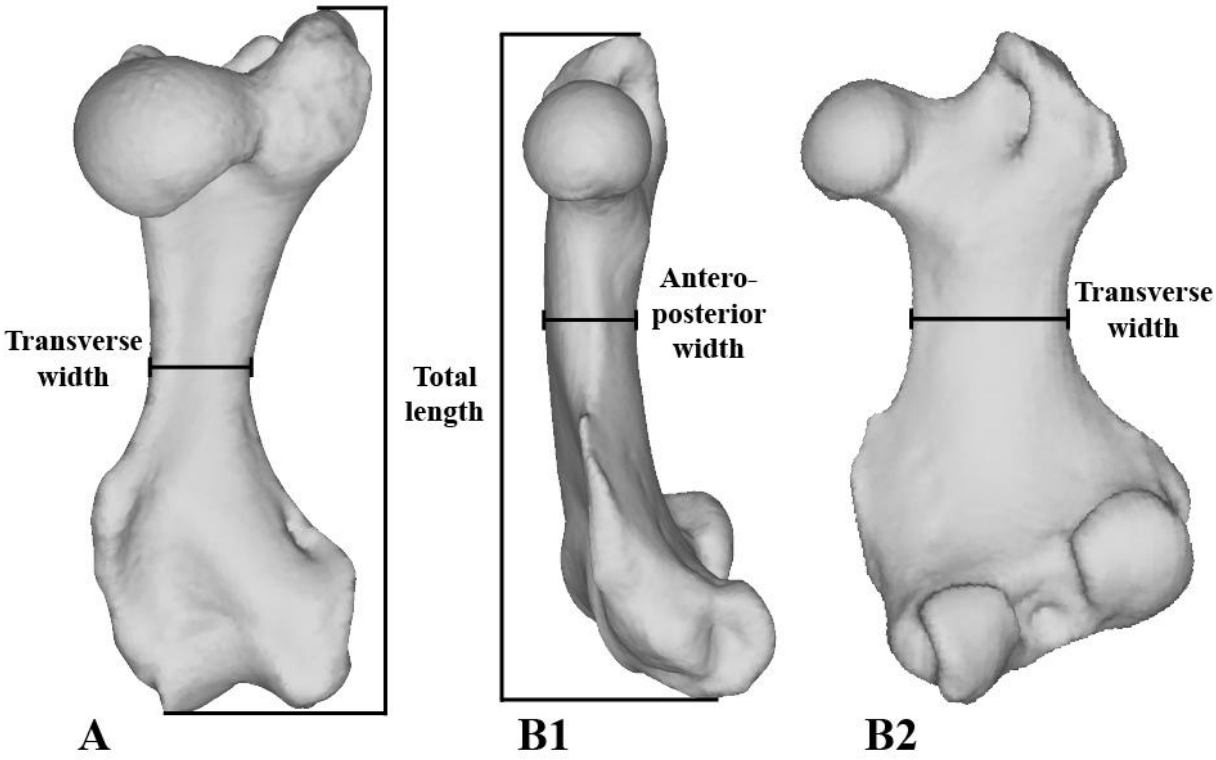

585

586 **Figure S3. Measurements of the length and width of the bones for computing *BI* index.**
587 **(**A) Measurements on the humerus, left humerus in posterior view; (B1) and (B2)
588 measurements on the femur, right femur in medial (B1), and posterior (B2) view.

589

Table S1. Taxon list. List presenting all the taxa presented in the present study, showing the provenance of the specimen(s) used in the present study for each taxon. For each locality and specimen(s), the associated age and depositional environment is listed too.

Taxon	Locality	Age
Cetacea (whales)		
Mysticeti (baleen whales)		
Cetotheriidae		
Brandtocetus sp.	Eastern Paratethys: South coast of Tobechik Lake, Kerch Peninsula, Crimea, Ukraine	Chersonian (= late Sarmatian s.l.), early Late Miocene (Tortonian)
Cetotheriinae indet.	Eastern Paratethys: South coast of Tobechik Lake, Kerch Peninsula, Crimea, Ukraine	Chersonian (= late Sarmatian s.l.), early Late Miocene (Tortonian)
Odontoceti (toothed whales)		
Cf. Platanistidae		
Pachyacanthus suessii	Central Paratethys: Nussdorf-Heiligenstadt, Vienna, Austria, and other localities from Vienna Basin; Leitha Mountains; Baranya and Nógrád counties, Hungary	Sarmatian s.s., late middle Miocene (late Serravallian)
Delphinida indet.	Central Paratethys: Bruckneudorf, Burgenland, Austria	Sarmatian s.s., late middle Miocene (late Serravallian)
Pinnipedia		
Phocidae (true seals)		
Cryptophoca maeotica	Central Paratethys: Hulbocica, Chisinau, Moldova	Middle to upper Bessarabian (= middle Sarmatian s.l.), earliest late Miocene, earliest Tortonian
Monachopsis pontica	Eastern Paratethys: Khroni Cape, north to Osoviny, Kerch peninsula, Crimea, Ukraine	Uppermost Chersonian (= late Sarmatian s.l.), just below the Sarmatian-Maeotian boundary. The consensus date for this boundary [S3] is between 7.4 and 7.5 Ma but Radionova et al. (2012) [S4] dates it as 8.69 Ma. => early late Miocene (late Tortonian)
Pachyphoca chapskii	Central Paratethys: Hulbocica, Chisinau, Moldova	Middle to upper Bessarabian (= middle Sarmatian s.l.), earliest late Miocene, earliest Tortonian
"*Phoca*" *bessarabica*	Central Paratethys: Hulbocica, Chisinau, Moldova	Middle to upper Bessarabian (= middle Sarmatian s.l.), earliest late Miocene, earliest Tortonian

Pontophoca sarmatica	Central Paratethys: Hulbocica, Chisinau, Moldova	Middle to upper Bessarabian (= middle Sarmatian s.l.), earliest late Miocene, earliest Tortonian
Praepusa sp.	Central Paratethys: Hulbocica, Chisinau, Moldova	Middle to upper Bessarabian (= middle Sarmatian s.l.), earliest late Miocene, earliest Tortonian
Sarmatonectes sintsovi	Central Paratethys: Hulbocica, Chisinau, Moldova	Middle to upper Bessarabian (= middle Sarmatian s.l.), earliest late Miocene, earliest Tortonian

Table S2. Morphometric data of phocid humeri. Measurements of the humeri of different extant and extinct Phocidae, used to quantify the presence or absence of pachyostosis at the level of the humerus. A high ratio (orange, red) points towards a higher thicker diaphysis and, hence, possibly pachyostosis compared to closely-related taxa. A lower ratio (green), the absence of pachyostosis. Note that, although a high ratio may suggest pachyostosis to be present in a given taxon, but does not guarantee it. Taxa of studied in the present study are indicated in bold. When subfamily identification has been inadequate in previous studies, it is indicated by a question mark. When subfamily identification is contested, it is considered uncertain. Abbreviation: subf., subfamily.

Taxon	Specimen number	Humerus		
		Total length (BL) (in mm)	Least transverse width diaphysis (TW) (in mm)	Ratio TW/BL
Extant Phocidae				
Cystophora cristata (subf. Phocinae)	USNM 188962	143,76	30,16	0,210
	USNM 504888	142,01	26,31	0,185
	USNM 504889	142,08	33,09	0,233
	USNM 504890	131,77	29,08	0,221
	USNM 572578	143,86	28,17	0,196
	USNM 572579	164,52	34,24	0,208
Erignathus barbatus (subf. Phocinae)	USNM 16116	155,24	23,43	0,151
	USNM 500250	153,47	24,24	0,158
	USNM 500251	152,01	25,08	0,165
Halichoerus grypus (subf. Phocinae)	USNM 197848	142,0	24,2	0,170
	USNM 446405	168,72	27,19	0,161
	USNM 446406	150,96	26,13	0,173
	USNM 504481	167,9	28,11	0,167
Hydrurga leptonyx (subf. Monachinae)	USNM 275208	172,45	36,57	0,212
	USNM 396931	171,38	38,56	0,225
	USNM 571676	185,93	38,02	0,204
Leptonychotes weddellii	USNM 550118	146,86	28,2	0,192

(subf. Monachinae)	USNM 550359	162,68	35,56	0,219
Monachus monachus (subf. Monachinae)	USNM 219059	146,54	24,58	0,168
Monachus schauinslandi (subf. Monachinae)	USNM 243839	135,85	27,5	0,202
	USNM 334577	123,31	26,15	0,212
Pagophilus groenlandicus (subf. Phocinae)	USNM 504476	119,32	22,82	0,191
	USNM 572634	109,15	19,07	0,175
	USNM 593976	135,96	22,82	0,168
Phoca vitulina (subf. Phocinae)	IRSNB 1157C	111	16,8	0,151
	IRSNB 1165S	109,6	16,2	0,148
	IRSNB 7605	110,4	18,0	0,163
	IRSNB 35247	110	15,2	0,138
	IRSNB 36548	122,9	18,8	0,153
Pusa sibirica (subf. Phocinae)	IRSNB 14210	75,7	10,0	0,132
	IRSNB 15264	79,4	11,8	0,149
	IRSNB 21170	74,7	10,9	0,146
	IRSNB 21171	91,4	12,6	0,138
	USNM 504941	85,5	11,6	0,136
Extinct Phocidae				
Batavipusa neerlandica (subf. Phocinae)	MAB 3798	64,9	11,8	0,182
Callophoca obscura (subf. Monachinae)	USNM 186944	150,6	27,8	0,185
	USNM 244047	153,13	27,1	0,177
	USNM 254327	152,1	29,7	0,195
	USNM 305263	146,4	25,3	0,173
	USNM 329031	144,9	26,8	0,185
	USNM 412266	163,87	29,99	0,183
	USNM 412296	138,3	24,1	0,174

	USNM 425705	154,43	22,4	0,145
	USNM 467713	147,75	24,8	0,168
Cryptophoca maeotica (subf. Phocinae?)	Average from [S10]	107,1	14,5	0,135
Leptophoca proxima (subf. Phocinae)	USNM 5359	124,5	14,9	0,120
	USNM 23450	113,4	13,5	0,119
	USNM 284721	126,2	15,0	0,119
	USNM 412115	131,7	14,4	0,109
Monachopsis pontica (subf. Phocinae?)	Average from [S11]	80,5	13,6	0,169
Nanophoca vitulinoides (subf. Phocinae)	IRSNB 1063-M242	78,2	9,5	0,121
	IRSNB M2276c	72,4	9,8	0,135
Pachyphoca ukrainica (subf. uncertain)	Average from [S12]	87,0	18,3	0,210
Phocanella pumilla (subf. Phocinae?)	USNM 171151	128,8	15,8	0,123
	USNM 305304	131,9	15,4	0,117
	USNM 329059	127,8	15,8	0,124
	USNM 421544	124,6	16,6	0,133
	USNM 437762	125,1	13,9	0,111
Praepusa boeska (subf. Phocinae?)	MAB 4686 (holotype)	81,1	11,3	0,139
Praepusa vindobonensis (subf. Phocinae)	Average from [S10]	86,3	10,6	0,123
Sarmatonectes sintsovi (subf. Phocinae?)	USNM unspecified plaster cast	90,4	13,9	0,154

Table S3. Morphometric data of phocid femora. Measurements of the femora of different extant and extinct Phocidae, used to quantify the presence or absence of pachyostosis at the level of the femur. A high ratio (orange, red) points towards a higher thicker diaphysis and, hence, possibly pachyostosis compared to closely-related taxa. A lower ratio (green), the absence of pachyostosis. Note that, although a high ratio may suggest pachyostosis to be present in a given taxon, but does not guarantee it. Taxa of studied in the present study are indicated in bold. When subfamily identification has been inadequate in previous studies, it is indicated by a question mark. When subfamily identification is contested, it is considered uncertain. Abbreviation: subf., subfamily.

Taxon	Specimen number	Femur			
		Total length (BL) (in mm)	Least transverse width diaphysis (TW) (in mm)	Anteroposterior thickness diaphysis (APW) (in mm)	Ratio [0.5*(TW+APW)]/BL
Extant Phocidae					
Cystophora cristata (subf. Phocinae)	USNM 188962	128,18	39,78	22,92	0,245
	USNM 572579	151,26	43,51	28,25	0,237
Erignathus barbatus (subf. Phocinae)	USNM 16116	149,14	34,14	20,09	0,182
	USNM 500250	151,37	35,48	20,95	0,186
	USNM 500251	136,65	36,33	19,47	0,204
Halichoerus grypus (subf. Phocinae)	USNM 197848	120,4	30,7	14,4	0,187
	USNM 446405	144,35	36,03	18,15	0,188
	USNM 446406	128,77	33,23	15,51	0,189
	USNM 504481	139,78	36,18	19,33	0,199
Hydrurga leptonyx (subf. Monachinae)	USNM 396931	141,4	39,9	26,1	0,233
	USNM 571676	150,8	41,2	24,1	0,216
Leptonychotes weddellii (subf. Monachinae)	USNM 550118	133,29	38,87	21,6	0,227
	USNM 550359	134,44	38,51	20,17	0,218
Monachus monachus (subf. Monachinae)	USNM 219059	123,56	33,98	22,94	0,23
Monachus schauinslandi (subf. Monachinae)	USNM 243839	103,26	30,28	17,43	0,231
	USNM 334577	91,01	28,03	19,77	0,263

Pagophilus groenlandicus (subf. Phocinae)	USNM 504476	112,06	29,69	17,1	0,209
	USNM 572634	97,04	27,38	15,2	0,219
	USNM 593976	115,12	32,76	15,23	0,208
Phoca vitulina (subf. Phocinae)	IRSNB 1157C	99,4	22,6	13,9	0,184
	IRSNB 7605	106,4	21,8	14	0,168
	IRSNB 35247	98,4	18,7	13,7	0,165
	IRSNB 36548	109,3	21,5	15,2	0,168
Pusa sibirica (subf. Phocinae)	IRSNB 14210	68,5	14,7	7,0	0,158
	IRSNB 15264	72,4	15,1	8,2	0,161
	IRSNB 21170	67,8	15,6	6,7	0,164
	IRSNB 21171	86,1	17,1	9,9	0,157
	USNM 504941	76,7	16,1	8,2	0,158
Extinct Phocidae					
Callophoca obscura (subf. Monachinae)	USNM 412294	130,22	40,31	24,32	0,24816
	USNM 412300	131,67	36,27	21,93	0,22101
	USNM 437849	124,26	37,12	22	0,23789
Cryptophoca maeotica (subf. Phocinae?)	Average from [S10]	106	27,6	12,4	0,189
Leptophoca proxima (subf. Phocinae)	USNM 263648	107,8	27	15,1	0,195
	USNM 347348	118,9	28,9	17,2	0,194
	USNM 559330	115,8	27,6	17	0,193
Monachopsis pontica (subf. Phocinae?)	Average from [S10]	68,3	18,1	9,7	0,204
Nanophoca vitulinoides (subf. Phocinae)	IRSNB1049-M246	73,6	19,8	9,7	0,200
	IRSNB M2271	71,5	20,3	9,5	0,208
	IRSNB M2276d	69,4	19,6	9,1	0,207
Pachyphoca chapskii (subf. uncertain)	NMNHU-P 64-706	120	33,5	21,5	0,229

Pachyphoca ukrainica (subf. uncertain)	Average from [S12]	80,3	24,3	14,3	0,240
Phocanella pumilla (subf. Phocinae?)	USNM 181649	124,1	29,5	15,9	0,183
	USNM 481569	115	27,4	12,3	0,173
Pontophoca sarmatica (subf. Monachinae?)	Average from [S11]	82,5	26,0	11,7	0,228
Praepusa vindobonensis (subf. Phocinae)	Average from [S10]	72,8	18,4	10,4	0,198
Sarmatonectes sintsovi (subf. Phocinae?)	PIN 1713/1352	89,5	21	13	0,190
	PIN 1713/140	94,5	22,5	13	0,188

Table S4. Compactness results.
Compactness of 2D cross sections of humeri, femora and ribs of extinct phocids and cetaceans from the Paratethys, compared with extant and extinct phocids and cetaceans in the literature. Compactness in the preset study calculated using Bone Profiler Version 4.5.8 [S13] and represented as a percentage of the overall surface area of the cross section. Data in bold represent the novel results in the present study. Daggers indicate extinct taxa.

Taxon	Source	Humerus %	Femur %	Rib %
Phocidae: main sample				
Cryptophoca maeotica†	This study	*ca*. 100	-	-
Monachopsis pontica†	This study	98.7	-	-
Pachyphoca chapskii†	This study	99.9	-	-
"*Phoca*" *bessarabica*†	This study	99.4	-	-
Pontophoca sarmatica†	This study	-	99.7	-
Praepusa† sp.	This study	-	98.5	-
Sarmatonectes sintsovi†	This study	99.3	-	-
Phocidae: comparative sample				
Callophoca obscura†	[S14]	-	59.1	-
Halichoerus grypus	[S14]	-	63.6	-
Leptophoca proxima†	[S14]	-	70.0	-
Mirunga leonina	[S15]	35.0	-	-
Nanophoca vitulinoides†	[S14]	-	99.4	-
Phoca vitulina	[S14]	-	52.0	-
Phocanella pumila†	[S14]	-	99.7	-
Cetacea: main sample				
Brandtocetus chongulek†	This study	-	-	*ca*. 100
Cetotheriidae† indet.	This study	-	-	99.8
Delphinida indet.	This study	99.4	-	-
Pachyacanthus suessii†	This study	-	-	99.9
Cetacea: comparative sample				
Basilosaurus† sp.	[S16]	-	98.9	84.9 - 95.2
Delphinapterus leucas	[S17]	-	-	85.8
Delphinus delphis (adult)	[S18,S19]	20.2 – 48.3	-	74.8

Dorudon atrox†	[S16]	-	98.8	61.3 – 96.1
Globicephala melas	[S17]	-	-	41.6
Inia goeffrensis	[S17]	-	-	36.5
Lissodelphis borealis	[S17]	-	-	74.3
Mesoplodon densirostris	[S17]	-	-	26.4
Monodon monoceros	[S18]	-	-	70.2
Orcinus orca	[S17]	-	-	87.9
Phocoena phocoena	[S18]	-	-	65.8
Qaisracetus†	[S16]	up to 92.5	-	-
Rodhocetus†	[S16]	-	87.4	73.9 – 91.6

Table S5. Osteohistological specimen list. Taxa and bones comprised in the main Paratethyan biological sample for the osteohistological part of the study. First hand observations and measurements were made on these specimens. Spot numbers refer to the map of Figures 1A and S1A and its caption. 'X' indicates that a thin section has been studied of a particular bone for a particular taxon. '-' indicates that it's not.

Taxon	Bone (use)			Spot
	Humerus	Femur	Rib	
PINNIPEDIA				
Phocinae (true seals)				
Cryptophoca maeotica	X	X	-	1
Monachopsis pontica	X	-	-	2
Pachyphoca chapskii	X	-	-	1
Pachyphoca ukrainica	-	X	-	1
"Phoca" bessarabica	X	-	-	1
Pontophoca sarmatica	-	X	-	1
Praepusa sp.	-	X	-	1
Sarmatonectes sintsovi	X	X	-	1
Sarmatonectes sintsovi	-	X	-	1
Sarmatonectes sintsovi	-	X	-	1
CETACEA				
MYSTICETI				
Cetotheriidae				
Brandtocetus chongulek	-	-	X	3
Cetotheriinae indet.	-	-	X	3
ODONTOCETI				
Delphinida				
Pachyacanthus suessii	-	-	X	4
Delphinida sp.	X	-	-	5

SUPPLEMENTAL REFERENCES

S1. Palcu, D.V., Tulbure, M., Bartol, M., Kouwenhoven, T.J., and Krijgsman, W. (2015). The Badenian–Sarmatian Extinction Event in the Carpathian foredeep basin of Romania: Paleogeographic changes in the Paratethys domain. Global Planet. Change *133*, 346-358.

S2. Kravciuk, I.P., Verina, V.N., and Suhov, I.M. (1976). Natural Reserves and Monuments of Moldova. Chisinau: Stiince. 309 p. [in Russian]

S3. Popov, S.V., Akhmetiev, M.A., Golovina, L.A., Goncharova, I.A., Radionova, E.P., Filippova, N.Y.U., and Trubichin, V.M. (2013). *Neogene regiostage stratigraphic scale of the South Russia: current state and perspectives*. 356–359. In: General stratigraphic scale of Russia. Current state and perspectives. Russian Conference. Moscow, 23–25 May 2013. GIN RAS, Moscow. [in Russian]

S4. Radionova, E.P., Golovina, L.A., Filippova, N.Y.U., Trubikhin, V.M., Popov, S.V., Goncharova, I.A., Vernigorova, Y.U.V., and Pinchuk, T.N. (2012). Middle-Upper Miocene stratigraphy of the Taman Peninsula, Eastern Paratethys. Cent. Eur. J. Geosci. *4*, 188-204.

S5. Vernyhorova, Y. (2015). Stratigraphic scheme for the Neogene deposits of the Northern Black Sea region and adjacent part of the Ukrainian Shield. Heolohiia ta rudonosnist Ukrainy *1*, 81-124. [in Ukrainian]

S6. Schmid, M.E. (1974). Faziostratotypus: Hernalser Tegel, Wien XVII, Hernals, Wiener Becken, Österreich. In M5 Sarmatien. Chronostratigraphie und Neostratotypen. Miozän der Zentralen Paratethys IV., A. Papp, F. Marinescu, and J. Seneš J, eds. (Bratislava: Vydavatel′stvo Slovenskej akadémie vied) pp. 168-170.

S7. Kazár, E. (2010). Revision of the genus *Pachyacanthus* Brandt, 1971 (Mammalia: Cetacea: Odontoceti). Ann. Naturhist. Mus. Wien, ser. *112*, 537-568.

S8. Nagel, D., Harzhauser, M., Rögl, F., Buttinger, R., Zetter, R., and Wanzenböck, G. (2007). Marines Knochenlager aus dem Mittelmiozän (Sarmat) des Wiener Beckens. Wiss. Mitt. Inst. Geol. TU Bergakad. Freiberg *36*, 102-103.

S9. Palcu, D.V., Golovina, L.A., Vernyhorova, Y.V., Popov, S.V., and Krijgsman, W. (2017). Middle Miocene paleoenvironmental crises in Central Eurasia caused by changes in marine gateway configuration. Global Planet. Change *158*, 57-71.

S10. Koretsky, I.A. (2001). Morphology and systematics of the Miocene Phocinae (Mammalia: Carnivora) from Paratethys and the North Atlantic region. Geol. Hun. Ser. Palaeontol. *54*, 1-109.

S11. Koretsky, I.A., and Grigorescu, D. (2002). The fossil monk seal *Pontophoca sarmatica* (Alekseev) (Mammalia: Phocidae: Monachinae) from the Miocene of eastern Europe. Sm. C. Paleob. *93*, 149-162.

S12. Koretsky, I.A., and Rahmat, S.J. (2013). First record of fossil Cystophorinae (Carnivora, Phocidae): middle Miocene seals from the northern Paratethys. Riv. Ital. Paleontol. S. *119*, 335-350.

S13. Girondot, M., and Laurin, M. (2003). Bone Profiler: a tool to quantify, model, and statistically compare bone section compactness profiles. J. Vertebr. Paleontol. *23*, 458-461.

S14. Quémeneur, S., Buffrénil, V. de, and Laurin, M. (2013). Microanatomy of the femur and inference of lifestyle in amniotes (Vertebrata, Tetrapoda). Biol. J. Linn. Soc. *109*, 644–655.

S15. Canoville, A., and Laurin, M. (2010). Evolution of humeral microanatomy and lifestyle in amniotes, and some comments on palaeobiological inferences. Biol. J. Linn. Soc. *100*, 384-406.

S16. Houssaye, A., Tafforeau, P., Muizon, C. de, and Gingerich, P. D. (2015). Transition of

Eocene whales from land to sea: evidence from bone microstructure. Plos One *10*, e0118409.

S17. Canoville, A., Buffrénil, V. de, and Laurin, M. (2016). Microanatomical diversity of amniote ribs: an exploratory quantitative study. Biol. J. Linn. Soc. *118*, 706-733.

S18. Buffrénil, V. de, Canoville, A., D'Anastasio, R., and Domning, D.P. (2010). Evolution of sirenian pachyosteosclerosis, a model-case for the study of bone structure in aquatic tetrapods. J. Mamm. Evol. *17*, 101-120.

S19. Buffrénil, V. de, and Schoevaert, D. (1988). On how the periosteal bone of the delphinid humerus becomes cancellous: ontogeny of a histological specialization. J. Morphol. *198*, 149-164.